

# UCLA

## UCLA Previously Published Works

### Title

Simultaneous T1 and B1+ Mapping Using Reference Region Variable Flip Angle Imaging

### Permalink

<https://escholarship.org/uc/item/81x7g6j3>

### Journal

Magnetic Resonance in Medicine, 70(4)

### ISSN

0740-3194

### Authors

Sung, Kyunghyun  
Saranathan, Manojkumar  
Daniel, Bruce L  
[et al.](#)

### Publication Date

2013-10-01

### DOI

10.1002/mrm.24904

Peer reviewed

Published in final edited form as:

*Magn Reson Med.* 2013 October ; 70(4): 954–961. doi:10.1002/mrm.24904.

## Simultaneous $T_1$ and $B_1^+$ Mapping using Reference Region Variable Flip Angle Imaging

Kyunghyun Sung<sup>1,\*</sup>, Manojkumar Saranathan<sup>2</sup>, Bruce L. Daniel<sup>2</sup>, and Brian A. Hargreaves<sup>2</sup>

<sup>1</sup>Department of Radiological Sciences, UCLA, Los Angeles, California, USA

<sup>2</sup>Department of Radiology, Stanford University, Stanford, California, USA

### Abstract

**Purpose**—To present a new method that can simultaneously and efficiently measure  $T_1$  and  $B_1^+$  maps using reference region variable flip angle (RR-VFA) imaging.

**Methods**—Assuming  $T_1$  relaxation time in a reference region such as fat is well characterized, and the reference region sufficiently covers smoothly varying  $B_1^+$  field inhomogeneity,  $B_1^+$  maps can be measured from VFA images, conventionally used for  $T_1$  measurements. Fat-only images from 2-point Dixon acquisitions were used to compute  $B_1^+$  maps, and the  $B_1^+$  maps were compared with ones using the double angle method (DAM) in 22 breast MRI patients at 3T. Additionally, high spatial resolution VFA images were acquired to show  $T_1$  measurements with and without the RR-VFA  $B_1^+$  correction in six patients.

**Results**—RR-VFA is able to generate reliable  $B_1^+$  maps, similar those using the conventional DAM. This simultaneous  $T_1$  and  $B_1^+$  mapping can also be used to reduce  $T_1$  estimation errors, where  $T_1$  maps have more uniform fibroglandular tissue  $T_1$  and better depiction of heterogeneous  $T_1$  of breast masses.

**Conclusion**—A new method that can measure both  $T_1$  and  $B_1^+$  maps based on Dixon VFA images is described, offering improved  $T_1$  quantification with no scan time penalty.

### Keywords

$B_1$  field inhomogeneity;  $T_1$  mapping; Quantitative DCE-MRI; Breast imaging; High-field MRI

## INTRODUCTION

Dynamic contrast-enhanced MRI (DCE-MRI) is a commonly used method in the diagnosis of cancer (1,2), which typically acquires a time series of T1-weighted images before and after injection of gadolinium contrast agent (CA). Pre-contrast  $T_1$  measurements are necessary to convert the signal intensities from T1-weighted images into CA concentration (3). CA uptake curves can be used to extract quantitative or semi-quantitative microvascular properties using pharmacokinetic modeling (4,5), which can potentially provide predictive, prognostic and pharmacodynamic response biomarkers for cancers (6–8).

One common method to measure  $T_1$  is variable flip angle (VFA) imaging, also known as Driven Equilibrium Single-Pulse Observation of T1 (DESPOT1), which uses several short TR spoiled gradient-echo (SPGR) acquisitions with varying flip angles (9–11). Using the SPGR signal equation and linear fitting,  $T_1$  maps can be estimated. VFA imaging is widely

\*Correspondence to: Kyunghyun Sung, PhD, Department of Radiological Sciences, 300 UCLA Medical Plaza, Suite B119, Los Angeles, CA 90095, Phone: (310) 267-6842, Fax: (310) 825-9118, ksung@mednet.ucla.edu.

used in DCE-MRI since it is highly time-efficient and allows rapid 3D volumetric  $T_1$  mapping with the same pulse sequence used to measure contrast uptake (9,12). Even though many efforts have been made to improve the accuracy of VFA imaging, VFA methods seem to be less accurate in vivo due to their high sensitivity to any flip angle variations (13–15).

Non-uniformity of transmit radiofrequency ( $B_1^+$ ) field can lead to flip angle variations from the prescribed flip angle. The  $B_1^+$  inhomogeneity tends to become more severe at higher field strengths. At 3 Tesla, noticeable  $B_1^+$  variations over the chest (around 30 – 50%) have been observed by many studies (16–19). Therefore, any  $B_1^+$  variation should be carefully addressed for any quantitative or multi-parametric imaging at 3T or higher field strengths, and the accuracy of VFA can be improved by compensating for the  $B_1^+$  variation (13,15,20).

Separate measurements of  $T_1$  and  $B_1^+$  prolong the clinical protocols. More importantly, many centers have limited ability to include time-efficient methods for  $B_1^+$  mapping, and there also exist previous  $T_1$  data without acquiring  $B_1^+$  mapping. Similar to VFA, the double-angle method (DAM) acquires images with two flip angles but requires long TRs ( $TR \gg T_1$ ) to avoid dependence on  $T_1$  (21), or requires a  $B_1$ -insensitive saturation pulse (17,22). In contrast, VFA intentionally includes the dependence of TR on  $T_1$  to compute  $T_1$  values without assuming any  $B_1^+$  variation. If  $T_1$  is known on a well-characterized and well-separated reference region (e.g., lipid tissue), the VFA signal equations can be used to estimate  $B_1^+$  variation in the reference tissue (23), and possibly, the entire  $B_1^+$  variation can be estimated by interpolating using the  $B_1^+$  variation in the reference tissue.

In this work, we describe a novel way to simultaneously measure  $T_1$  and  $B_1^+$  maps using reference region VFA (RR-VFA) imaging. Assuming the  $T_1$  relaxation time for breast fat tissue (reference region) is globally uniform and well characterized at 3T (24), we use a two-point Dixon algorithm (25) to generate fat-only images and assign a known fat  $T_1$  value to a ratio of signal magnitudes for computing  $B_1^+$  variation. Secondly, assuming the  $B_1^+$  field inhomogeneity is smoothly varying across the breast (15,18,19), we apply 3D interpolation to construct the complete  $B_1^+$  variation map. We then compare our  $B_1^+$  maps with those using conventional DAM in 22 breast MRI patients and show differences in  $T_1$  calculation with and without compensating for the  $B_1^+$  variation in six breast MRI patients at 3T.

## METHODS

The signal intensity ( $I_{\alpha_n}$ ) using SPGR with a nominal flip angle ( $\alpha_n$ ) can be expressed as:

$$I_{\alpha_n} = M_0 \frac{(\sin \alpha_n (1 - E_1))}{(1 - E_1 \cos \alpha_n)}, \quad [1]$$

where  $M_0$  is the longitudinal magnetization including coil sensitivities and  $E_1 = e^{-TR/T_1}$ . Introducing a relative flip angle variation  $B_f(r)$ , defined by a ratio between the actual flip angle and the prescribed flip angle (i.e., 1 means the actual flip angle is same as the prescribed flip angle, and 0.5 means 50% reduction in the flip angle), we can express the actual flip angle as  $B_f(r)\alpha_n$ . A signal ratio of signal magnitudes with two flip angles ( $\alpha_1$  and  $\alpha_2$ ) for each voxel can be written as:

$$\frac{I_{\alpha_2}(r)}{I_{\alpha_1}(r)} = \frac{\sin(B_1(r)\alpha_2) \cdot (1 - E_1 \cos(B_1(r)\alpha_1))}{\sin(B_1(r)\alpha_1) \cdot (1 - E_1 \cos(B_1(r)\alpha_2))}, \quad [2]$$

where  $r$  represents spatial position. Provided the fat  $T_1$  is known and is globally uniform,  $B_f(r)$  in fatty tissue ( $r$  in the reference region) becomes the only unknown in Eq. [2] and can be numerically calculated using the signal ratio for each voxel. Note that any image non-

uniformities (e.g., receive sensitivity) except for the flip angle variation are cancelled out, as they are identical for both magnitude images.

We investigated the accuracy of the RR-VFA  $B_1^+$  measurement with different sets of flip angles and different signal-to-noise ratios (SNRs) using numerical simulations. We simulated fat signal as a function of relative flip angle variation  $B_1$  (from 0.2 to 1.8), based on a published value for fat  $T_1$  of 367 ms (24). To account for any inaccuracies between true and assumed  $T_1$  values in the reference region, we also examined possible  $B_1^+$  measurement errors when there exist variations of the reference region  $T_1$  value. With TR of 4 ms, the Ernst angle for the fat signal was  $8.5^\circ$ . Three sets of signal ratios ( $5^\circ/10^\circ$ ,  $10^\circ/15^\circ$ , and  $5^\circ/15^\circ$ ) were selected to evaluate the signal behavior, and three different noise levels were added to the simulated signal (maximum SNRs were 12, 26 and 74). The accuracy of the estimated  $B_1$  was analyzed using second order statistics: mean and standard deviation (SD).

Figure 1 illustrates the method of generating a final  $B_1^+$  map using RR-VFA. After computing the signal ratio of two fat-only signal magnitudes, we computed a fat-only relative flip angle map using the numerically simulated signal ratio. When the fat-water separation is not perfect, partial-volume effects can cause an error in the flip angle map due to additional  $T_1$  values. This can be reduced by enforcing a smoothing constraint using a quadratic penalty:

$$f(r) = \frac{1}{n_r} \sum_{p \in \delta_r} (B_1(r) - B_1(p))^2, \quad [3]$$

where  $\delta_r$  is the 3rd-order neighborhood only in the fatty tissue (which, in three dimensions, includes the maximum of 124 voxels ( $5 \times 5 \times 5$  boxcar) surrounding  $p$ ), and  $n_r$  is a total number of voxels in  $\delta_r$ . We excluded the spatial location  $r$  in the flip angle map when the penalty function  $f(r)$  becomes more than 0.04.

Secondly, we applied 3D interpolation and reduced the spatial resolution to fill up the non-fat region. The interpolation method fits a surface of the measured fat-only region to the entire three-dimensional data using the *griddata* function in Matlab (R2012b; The Mathworks, Natick, MA). The fitting was based on linear interpolation, but other fitting methods can also be applied. We reduced the spatial resolution by a factor of two in all three directions by applying a Gaussian window in the frequency domain, assuming that  $B_1^+$  field inhomogeneity varies smoothly across the object (15,18,19).

Experiments were performed on 3.0T GE MR 750 systems (GE Healthcare, Waukesha, WI). The axial orientation was chosen for all imaging as it is commonly used in breast MRI, and a large  $B_1^+$  variation is expected from left to right. A body coil was used for  $B_1$  transmission, and the automatic pre-scan values provided by the scanner were used to calibrate  $B_1$  transmission. No transmit RF field shimming is used. This retrospective review and analysis of the VFA data was performed in accordance with a protocol approved by our Institutional Review Board.

The VFA sequence was performed as a part of our standard clinical breast DCE-MRI protocol. We analyzed data on a total of 22 women undergoing clinically indicated breast MRI for a history of known or suspected breast disease, ranging in age between 26 and 73 years (age =  $49.9 \pm 11.2$  years and mass =  $60.9 \pm 7.4$  kg). Based on the official mammographic breast density, rated on a scale of four: fatty (F), scattered fibroglandular densities (S), heterogeneously dense (H), and dense (D), the 22 cases were classified as 6 S, 7 H, and 2 D, with 7 not being assigned. We used a 3D SPGR sequence with a dual-echo bipolar readout, where TEs were chosen to be in- and opposed-phase images (TE = 1.2/2.4

ms), and a two-point Dixon fat-water separation algorithm was used to generate fat- and water-only images (25). We performed the  $T_1$  mapping before DCE-MRI using two flip angles of  $6^\circ$  and  $13^\circ$ , optimized to symmetrically sample the signal curve of fat ( $T_1$  was assumed to be 367 ms (24) and  $TR = 4.3$  ms in simulation). Other imaging parameters were as follows: acquisition matrix size =  $256 \times 128 \times 88$ , slice thickness = 4.2 mm, FOV = 32 cm, and total scan time = 20 sec.

For comparison of  $B_1^+$  measurements, we also measured  $B_1^+$  maps using conventional DAM (21) and used the Bland-Altman plot to show the differences between two  $B_1^+$  mapping methods in 22 subjects. We acquired the  $B_1^+$  maps after post contrast scans to ensure greater  $T_1$  relaxation recovery of all tissue with flip angles of  $60^\circ$  and  $120^\circ$  and  $TR$  of 5 sec. Errors due to imperfect 2D slice profiles were corrected in the flip angle calculation (26). We normalized an actual flip angle map by  $60^\circ$  to compute the relative flip angle variation. Other imaging parameters were as follows: echo time (TE) = 2.5 ms, acquisition matrix =  $64 \times 64$ , number of slices = 49, slice thickness = 4 mm, field-of-view (FOV) = 44 cm, and total scan time = 9 min.

Lastly, in six additional breast patient cases (age =  $52.2 \pm 10.4$  years and mass =  $76.5 \pm 13.7$  kg), we acquired data with more than two flip angles using high spatial resolution VFA imaging to measure simultaneous  $T_1$  and  $B_1^+$  maps. We used the same dual-echo bipolar readout and selected five flip angles of  $2^\circ$ ,  $5^\circ$ ,  $9^\circ$ ,  $13^\circ$ , and  $15^\circ$ , optimized to symmetrically sample the signal curve of the fibroglandular tissue  $T_1$ . We used  $5^\circ$  and  $15^\circ$  fat-only images for  $B_1^+$  maps and used all five flip angles for  $T_1$  maps with compensation for the  $B_1^+$  variation. Other imaging parameters were as follows: acquisition matrix size =  $262 \times 308 \times 192$ , slice thickness = 1.2 mm,  $TR = 4.3$ , FOV = 32 cm, and total scan time = 7 min 25 sec.

## RESULTS

### Numerical Simulation

Figure 2a shows fat signal intensity  $I_a$  (mean and SD) as a function of relative flip angle variation with different nominal flip angles ( $\alpha = 5^\circ, 10^\circ$  and  $15^\circ$ ). We added the same level of Gaussian noise to the simulated signal, accounting for error bars in the plots, and the nominal SNRs (SNRs with no  $B_1^+$  variation) for  $5^\circ, 10^\circ$  and  $15^\circ$  were 21, 26, and 21 respectively. Among all three types of signal ratios, the signal ratio of  $5^\circ$  and  $15^\circ$  ( $I_5/I_{15}$ ) has the biggest dynamic range with the lowest SD (Fig 2b), possibly resulting in the lowest estimation error. Fig 2c shows the plots between the estimated and true flip angle variation, indicating the estimation error using the signal ratio (Eq. [2]). The solid gray lines are the identity lines. For  $I_5/I_{15}$ , the mean of the estimated  $B_1$  becomes very close to the true  $B_1$  with very small SD (SD/mean ranges from 0.6 to 0.8) when the true  $B_1$  is between 0.6 and 1.4, a typical range of  $B_1^+$  variation for breast imaging at 3T (15,18,19).

Figure 3 illustrates the accuracy of the proposed  $B_1^+$  measurement with different SNRs. Three different levels of Gaussian noise have been added to the simulated fat signal, and the nominal SNRs for  $15^\circ$  were 11, 21, and 66. When SNR is extremely low (e.g., less than 15), the measurement becomes slightly biased with the significant noise sensitivity, especially around the high  $B_1^+$  variation range ( $\pm 40\%$ ). However, when SNR is marginal (e.g., more than 30), the measurement does not include any systematic bias with the very low measurement SD (i.e., high accuracy and high precision). Note that we can typically expect sufficient SNRs for VFA imaging due to the short  $T_1$  of fat.

Figure 4 shows the effects of assumed reference region  $T_1$  values on the RR-VFA  $B_1^+$  estimation for a true  $T_1$  value of 367 and 1200 ms. When there exists any difference between

the true and assumed  $T_1$  values in the reference region, the numerical signal ratio (Eq. [2]) becomes different from the true signal ratio, and the RR-VFA  $B_1^+$  estimation can be less accurate. Fig 4a shows different signal ratios for  $\pm 5\%$  variations of the true short  $T_1$  ( $367 \pm 18$  ms) and long  $T_1$  ( $1200 \pm 60$  ms) values. When the assumed reference region  $T_1$  is longer than the true  $T_1$ , the proposed method typically underestimates  $B_1^+$  variation, resulting in negative percentage errors, while the shorter  $T_1$  results in positive percentage errors. Fig 4b shows the  $B_1^+$  estimation errors caused by these  $T_1$  variations. Within  $\pm 5\%$  variations of the true  $T_1$ , the difference in the signal ratios is subtle, and the  $B_1^+$  estimation error is well within  $\pm 2.5\%$ . Furthermore, with  $\pm 10\%$  and  $\pm 15\%$  variations of the true  $T_1$ , the  $B_1^+$  estimation errors are around  $\pm 5\%$  and  $-7$  to  $+8\%$  for both short and long  $T_1$  values.

### Comparison between RR-VFA and DAM

Figure 5 shows examples of  $B_1^+$  maps, shown as relative flip angle distribution (%), in subjects with heterogeneously dense (Fig 5a) and dense (Fig 5b) breasts using DAM and RR-VFA. Among the four levels of breast density rated based on the mammogram reports (fatty, scattered fibroglandular densities, heterogeneously dense, and dense), those two cases were considered to include the least amount of the fatty tissue. The  $B_1^+$  maps using two different methods are qualitatively well matched with each other. There exists a small region in the heart that shows a slight disagreement between two methods (see the arrows) because the heart does not include enough fatty tissue, but the heart was not the tissue of interest in our study. In all 22 cases, the proposed method was able to robustly generate  $B_1^+$  maps, qualitatively well matched with those using DAM. Note that 3D imaging was used for RR-VFA, whereas multi-slice 2D imaging was used for DAM.

Figure 6 shows the mean and SD of relative  $B_1^+$  variation over the region of interest (ROI) for a single subject (Fig 6a and b), and the Bland-Altman plot comparing the  $B_1^+$  maps over the ROI measured by RR-VFA and DAM in 22 subjects (Fig 6c). We manually defined circular ROIs almost covering each of the whole left and right breasts in the central axial slice. Both methods show similar patterns (mean  $\pm$  SD) of  $B_1^+$  variation within each breast, and the difference in  $B_1^+$  variation is very small (the 95% confidence interval is ranging from  $-8.9\%$  to  $3\%$ ).

### Simultaneous $T_1$ and $B_1^+$ mapping using RR-VFA

Figure 7 shows representative high spatial resolution  $T_1$  and  $B_1^+$  maps including both fat and fibroglandular tissue. The “water+fat” image is shown in Fig 7a. The  $T_1$  map using conventional VFA imaging, generated by the nominal flip angle of  $2^\circ$ ,  $5^\circ$ ,  $9^\circ$ ,  $13^\circ$ , and  $15^\circ$ , has considerable  $T_1$  differences between the left and right breast (shown in Fig 7b), while the high spatial resolution  $T_1$  map using RR-VFA shows more uniform fibroglandular  $T_1$  across the whole breast (shown in Fig 7d) and better depicts heterogeneous  $T_1$  of several breast masses (see the arrows). We used the  $5^\circ$  and  $15^\circ$  fat-only images for  $B_1^+$  mapping and all five flip angles (water+fat images) for  $T_1$  mapping with compensation for the  $B_1^+$  variation.

Figure 8 shows box plots (median, 25th and 75th percentiles, and lower and upper extremes) of fibroglandular  $T_1$  estimation using VFA and RR-VFA in all six patients. The estimated fibroglandular  $T_1$  values using VFA (without  $B_1^+$  correction) are  $1607.3 \pm 343.8$  ms (mean  $\pm$  SD) on the left ROI and  $799.4 \pm 191.2$  ms on the right ROI, while the estimated glandular  $T_1$  values using RR-VFA (with  $B_1^+$  correction) are  $1262.8 \pm 37.2$  ms on the left ROI and  $1304.0 \pm 104.5$  ms on the right ROI. The  $T_1$  difference between the left and right fibroglandular ROIs is 50% and is reduced to 3% after correcting for the  $B_1^+$  variation.

## DISCUSSION

For simultaneous  $T_1$  and  $B_1^+$  mapping, the proposed method (RR-VFA) relies on two major assumptions: the  $T_1$  value of the reference region is known, and the reference region sufficiently covers the smoothly varying  $B_1^+$  inhomogeneity across the object. With those two assumptions, we were able to measure  $B_1^+$  maps in the reference region (i.e., fatty tissue) and to estimate  $T_1$  maps over the non-reference region (i.e., non-fatty tissue). Furthermore, the proposed method naturally allows improved accuracy of the  $T_1$  estimation by accounting for the estimated  $B_1^+$  variation.

The first major assumption for the proposed method is that the  $T_1$  value for the fatty tissue is globally uniform and well-characterized. For breast fat, the previous study has shown  $T_1$  values are very consistent ( $366.8 \pm 7.8$  ms) across five healthy women at 3T (24), especially when the fat and water separation was performed using IDEAL (27). For subcutaneous fat, another study has also shown consistent  $T_1$  values ( $382 \pm 13$  ms) across six healthy volunteers at 3T (28). In these studies, the fat  $T_1$  values are fairly consistent and well within a range of  $\pm 5\%$  variation, where we have shown the proposed method is robust to these  $T_1$  variations. However, there may exist some systematic bias in the fat  $T_1$  measurements largely because different studies have used different measurement methods, especially with and without fat-water separation. Therefore, we believe it is important to carefully verify the assumed fat  $T_1$  to avoid any systematic  $T_1$  bias when different  $T_1$  measurement methods are used in RR-VFA.

The second assumption is that the fatty tissue sufficiently covers the smoothly varying  $B_1^+$  inhomogeneity across the object. This is generally true for breast imaging, but populations who have dense breasts may not have enough fatty tissue to represent the smooth  $B_1^+$  variation across the breasts. In this study, we included 8 heterogeneously dense and 2 dense breast cases but did not find any cases with extremely negligible fatty tissue. This may restrict the use of this method for imaging in other parts of the body. However, recent study also showed  $B_1^+$  variation can be described by a small set of basis (Bessel/Fourier) functions (29), suggesting that even a small reference region can still be effective for  $B_1^+$  mapping if the reference region is well distributed across the object of interest.

We used a two-point Dixon method to identify the fatty tissue in the breast for  $B_1^+$  mapping. We expect other Dixon-based methods (e.g., IDEAL) to yield better fat-water separation, which can reduce fat-water partial volume effects (27). If fat-water separation methods are not available, a manual or semi-manual segmentation method may be alternatively used to locate the pure fat-only region. However, if conventional fat saturation were applied for VFA images, the proposed method would not be directly applicable, since it is not possible to locate the fatty tissue.

Conventional DAM is well known to have a limited dynamic range for reliable  $B_1^+$  measurements (17,21,22). In fact, DAM  $B_1^+$  estimation becomes less reliable when the measured relative  $B_1^+$  variation becomes smaller (i.e., the actual flip angle is smaller than the prescribed flip angle) due to increased noise sensitivity (17). Although we corrected the errors due to an imperfect 2D slice profile for DAM, there may exist other errors, which can be more significant in the right breast than the left breast since the actual flip angles in the right breast are typically lower than the actual flip angles in the left breast (15,19). Nevertheless, both DAM and RR-VFA methods have similar  $B_1^+$  estimates over the breast at 3T.

To measure  $B_1^+$  variation, we have exploited the breast fat tissue as a reference region because the  $T_1$  value of fat is well characterized and is known to be consistent across the different subjects. However, it may be possible to use other tissue as the reference region in

this method, if it has well-characterized  $T_1$  values (e.g., saline implants, pelvic muscle etc), but the reliability of  $B_1^+$  mapping may vary.

The VFA imaging is commonly used in routine clinics to calculate  $T_1$ , especially as a part of DCE-MRI protocols. One advantage of the proposed technique is to allow generation of  $B_1^+$  maps in addition to  $T_1$  maps without additional scanning and without much change to the existing protocol. This may alleviate concerns of being its clinical protocol to be time-efficient, and it can also be easier to employ the technique without seeking any options for time-efficient methods for  $B_1^+$  mapping. More importantly, as long as the two main assumptions are satisfied, we can retrospectively correct for  $B_1$  effects in  $T_1$  estimation in previously acquired data sets, which did not include  $B_1^+$  mapping.

## CONCLUSION

We have described a novel method that can efficiently measure both  $T_1$  and  $B_1^+$  maps when a constant- $T_1$  reference region is available. The proposed method uses Dixon variable flip angle imaging, and  $B_1^+$  maps are computed based on two major assumptions: the  $T_1$  value of fat tissue is uniform and consistent across patients, and the fat region sufficiently covers the smoothly varying  $B_1^+$  inhomogeneity across the region of interest. We have shown  $B_1^+$  maps using the proposed method are similar to those using the conventional DAM and compensating for  $B_1^+$  variation using RR-VFA can reduce  $T_1$  estimation errors.

## Acknowledgments

### Grant Sponsors:

NIH R01-EB009055

## References

1. Kuhl C. MRI of breast tumors. *European radiology*. 2000; 10:46–58. [PubMed: 10663717]
2. Hayes C, Padhani AR, Leach MO. Assessing changes in tumour vascular function using dynamic contrast-enhanced magnetic resonance imaging. *NMR in Biomedicine*. 2002; 15:154–163. [PubMed: 11870911]
3. Schabel MC, Parker DL. Uncertainty and bias in contrast concentration measurements using spoiled gradient echo pulse sequences. *Phys Med Biol*. 2008; 53:2345–2373. [PubMed: 18421121]
4. Tofts PS, Brix G, Buckley DL, Evelhoch JL, Henderson E, Knopp MV, Larsson HBW, Lee T-Y, Mayr NA, Parker GJM. Estimating Kinetic Parameters From Dynamic Contrast-Enhanced T1-Weighted MRI of a Diffusible Tracer: Standardized Quantities and Symbols. *J Magn Reson Imaging*. 1999; 10:223–232. [PubMed: 10508281]
5. Evelhoch JL. Key Factors in the Acquisition of Contrast Kinetic Data for Oncology. *J Magn Reson Imaging*. 1999; 10:254–259. [PubMed: 10508284]
6. Esserman L, Hylton N, Yassa L, Barclay J, Frankel S, Sickles E. Utility of magnetic resonance imaging in the management of breast cancer: evidence for improved preoperative staging. *Journal of clinical oncology*. 1999; 17:110–110. [PubMed: 10458224]
7. Hawighorst H, Weikel W, Knapstein PG, Knopp MV, Zuna I, Schönberg S, Vaupel P, van Kaick G. Angiogenic activity of cervical carcinoma: assessment by functional magnetic resonance imaging-based parameters and a histomorphological approach in correlation with disease outcome. *Clinical cancer research*. 1998; 4:2305–2312. [PubMed: 9796959]
8. Zahra MA, Hollingsworth KG, Sala E, Lomas DJ, Tan LT. Dynamic contrast-enhanced MRI as a predictor of tumour response to radiotherapy. *The Lancet Oncology*. 2007; 8:63–74. [PubMed: 17196512]
9. Deoni SCL, Rutt BK, Peters TM. Rapid combined T1 and T2 mapping using gradient recalled acquisition in the steady state. *Magn Reson Med*. 2003; 49:515–526. [PubMed: 12594755]



10. Brookes JA, Redpath TW, Gilbert FJ, Murray AD, Staff RT. Accuracy of T1 measurement in dynamic contrast-enhanced breast MRI using two-and three-dimensional variable flip angle fast low-angle shot. *J Magn Reson Imaging*. 1999; 9:163–171. [PubMed: 10077009]
11. Zhu X, Li K, Kamaly-Asl I, Checkley D, Tessier J, Waterton J, Jackson A. Quantification of endothelial permeability, leakage space, and blood volume in brain tumors using combined T1 and T2\* contrast-enhanced dynamic MR imaging. *J Magn Reson Imaging*. 2000; 11:575–585. [PubMed: 10862055]
12. Wang HZ, Riederer SJ, Lee JN. Optimizing the precision in T1 relaxation estimation using limited flip angles. *Magn Reson Med*. 1987; 5:399–416. [PubMed: 3431401]
13. Treier R, Steingoetter A, Fried M, Schwizer W, Boesiger P. Optimized and combined T1 and B1 mapping technique for fast and accurate T1 quantification in contrast-enhanced abdominal MRI. *Magn Reson Med*. 2007; 57:568–576. [PubMed: 17326175]
14. Deoni SC. High-resolution T1 mapping of the brain at 3T with driven equilibrium single pulse observation of T1 with high-speed incorporation of RF field inhomogeneities (DESPOT1-HIFI). *J Magn Reson Imaging*. 2007; 26:1106–1111. [PubMed: 17896356]
15. Sung K, Daniel BL, Hargreaves BA. Transmit B1+ field inhomogeneity and T1 estimation errors in breast DCE-MRI at 3 Tesla. *J Magn Reson Imaging*. 2013; 1002/jmri.23996
16. Greenman RL, Shirosky JE, Mulkern RV, Rofsky NM. Double Inversion Black-Blood Fast Spin-Echo Imaging of the Human Heart: A Comparison Between 1.5T and 3.0T. *J Magn Reson Imaging*. 2003; 17:648–655. [PubMed: 12766893]
17. Sung K, Nayak KS. Measurement and characterization of RF nonuniformity over the heart at 3T using body coil transmission. *J Magn Reson Imaging*. 2008; 27:643–648. [PubMed: 18306272]
18. Kuhl CK, Kooijman H, Gieseke J, Schild HH. Effect of B1 inhomogeneity on breast MR imaging at 3.0 T. *Radiology*. 2007; 244:929–930. [PubMed: 17709843]
19. Azlan CA, Di Giovanni P, Ahearn TS, Semple SIK, Gilbert FJ, Redpath TW. B1 transmission-field inhomogeneity and enhancement ratio errors in dynamic contrast-enhanced MRI (DCE-MRI) of the breast at 3T. *J Magn Reson Imaging*. 2010; 31:234–239. [PubMed: 20027594]
20. Di Giovanni P, Azlan C, Ahearn T, Semple S, Gilbert F, Redpath T. The accuracy of pharmacokinetic parameter measurement in DCE-MRI of the breast at 3 T. *Physics in Medicine and Biology*. 2010; 55:121. [PubMed: 20009182]
21. Insko, EK.; Bolinger, L. B1 mapping. *Proc, SMRM, 11th Annual Meeting; Berlin*. 1992. p. 4302
22. Cunningham CH, Pauly JM, Nayak KS. SDAM: Saturated double angle method for rapid B1+ mapping. *Magn Reson Med*. 2006; 55:1326–1333. [PubMed: 16683260]
23. Gupta, SN.; Schmidt, EJ.; Mulkern, R.; Fedorov, A.; Hancu, I.; Zhu, Y.; Tempany-Afdhal, C.; Fennessy, F. A Method for Correcting T1 maps of Prostate at 3T Obtained by Variable Flip Angle Imaging. *Proc, ISMRM, 20th Annual Meeting; Melbourne*. 2012. p. 1962
24. Rakow-Penner R, Daniel B, Yu H, Sawyer-Glover A, Glover GH. Relaxation times of breast tissue at 1.5 T and 3T measured using IDEAL. *J Magn Reson Imaging*. 2006; 23:87–91. [PubMed: 16315211]
25. Ma J. Breath-hold water and fat imaging using a dual-echo two-point dixon technique with an efficient and robust phase-correction algorithm. *Magn Reson Med*. 2004; 52:415–419. [PubMed: 15282827]
26. Schär M, Vonken EJ, Stuber M. Simultaneous B0- and B1+-map acquisition for fast localized shim, frequency, and RF power determination in the heart at 3 T. *Magn Reson Med*. 2010; 63:419–426. [PubMed: 20099330]
27. Reeder SB, Pineda AR, Wen Z, Shimakawa A, Yu H, Brittain JH, Gold GE, Beaulieu CH, Pelc NJ. Iterative decomposition of water and fat with echo asymmetry and least-squares estimation (IDEAL): application with fast spin-echo imaging. *Magn Reson Med*. 2005; 54:636–644. [PubMed: 16092103]
28. de Bazelaire CM, Duhamel GD, Rofsky NM, Alsop DC. MR imaging relaxation times of abdominal and pelvic tissues measured in vivo at 3.0 T: preliminary results. *Radiology*. 2004; 230:652–659. [PubMed: 14990831]
29. Sbrizzi A, Hoogduin H, Lagendijk JJ, Luijten P, van den Berg CA. Robust reconstruction of B1+ maps by projection into a spherical functions space. *Magn Reson Med*. 2013; 1002/mrm.24640

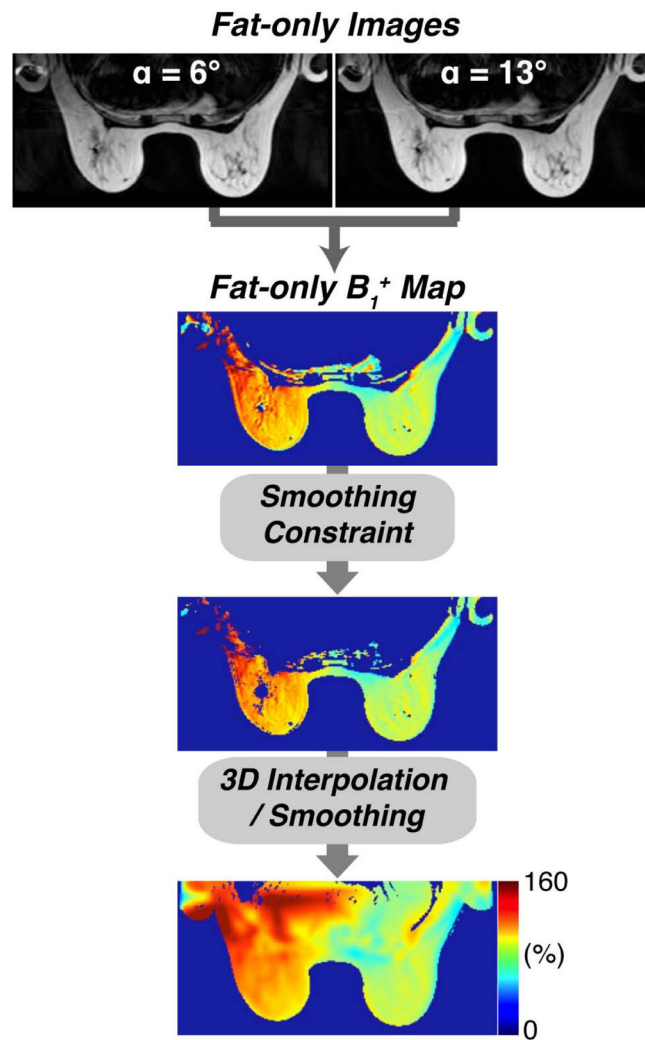


**Figure 1.** A diagram of the proposed B<sub>1</sub><sup>+</sup> mapping using RR-VFA. After computing a fat-only B<sub>1</sub><sup>+</sup> map using the signal ratio of two fat-only images, the proposed method applies a smoothing constraint and 3D interpolation to construct the complete B<sub>1</sub><sup>+</sup> map.

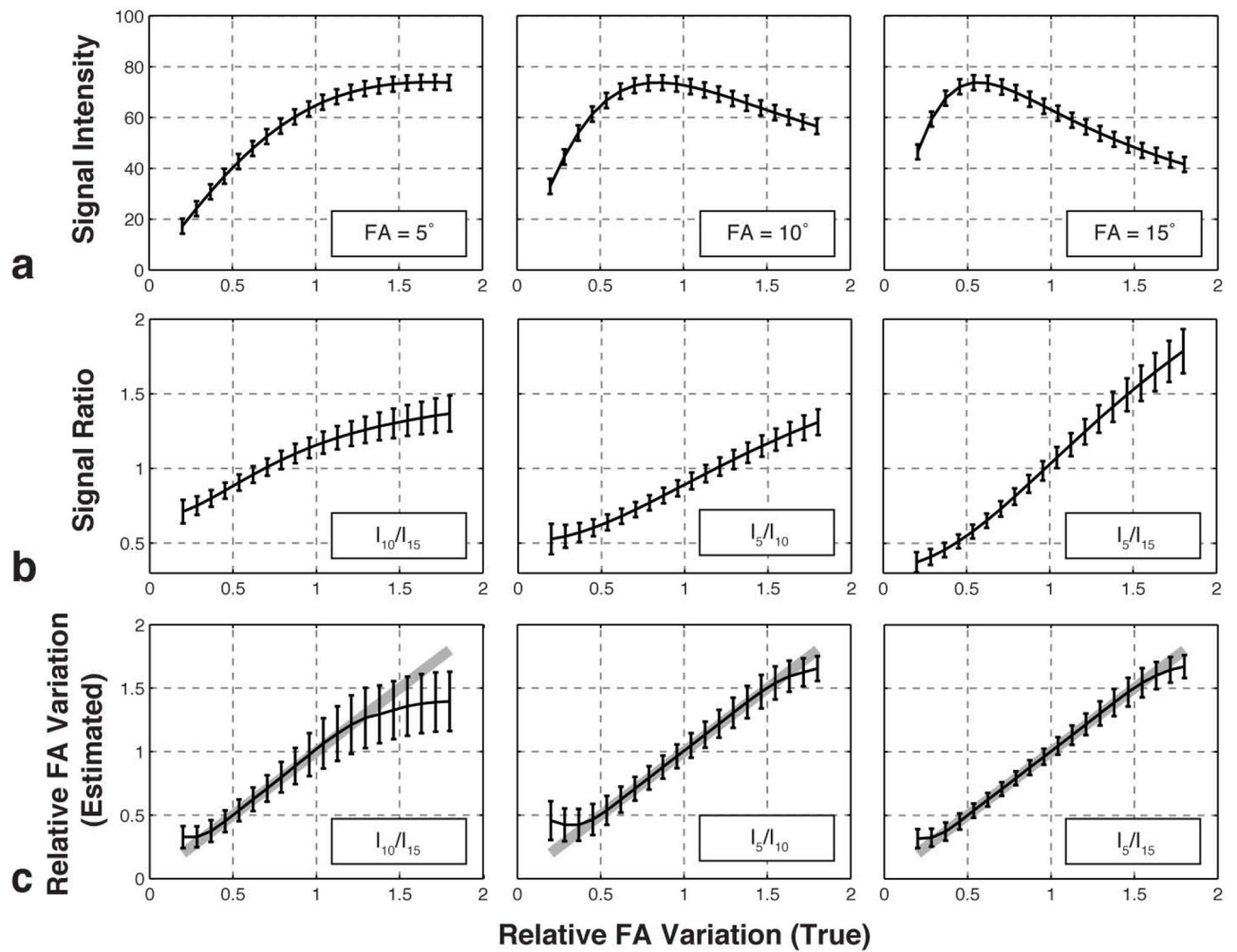


**Figure 2.** Signal behavior of fat with (a) differing flip angles (5°, 10° and 15°) and (b) differing signal ratios ( $I_{10}/I_{15}$ ,  $I_5/I_{10}$  and  $I_5/I_{15}$ ), and (c) plots between the estimated and true flip angle variation for differing signal ratios (solid gray lines are the identity line). We added the same level of Gaussian noise to the simulated signal, and the plots are expressed as mean  $\pm$  SD.

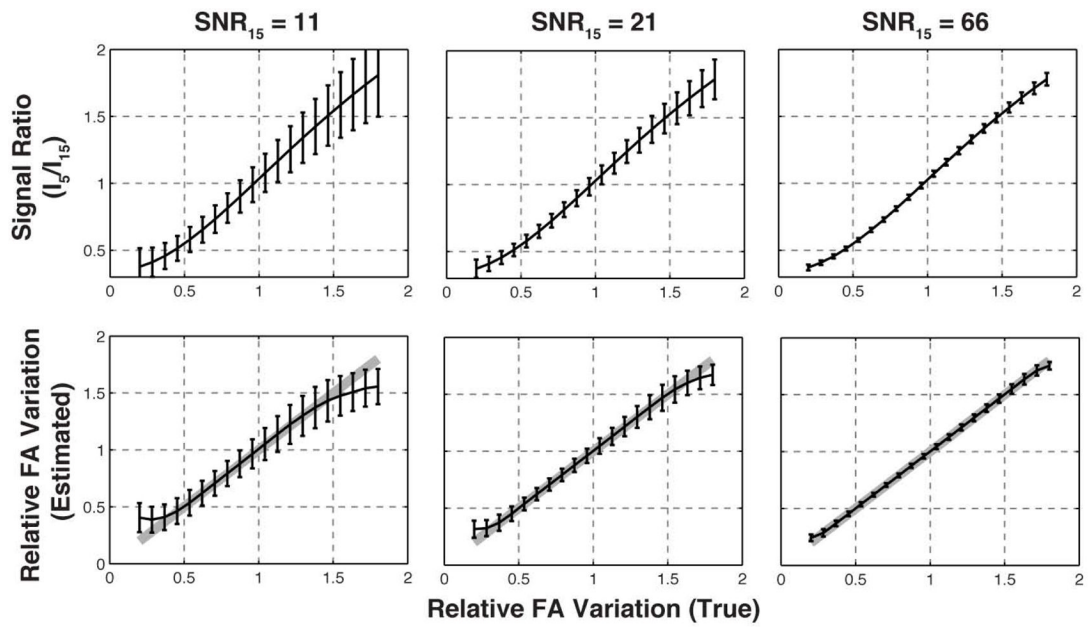


**Figure 3.** Measurement accuracy of the RR-VFA  $B_1^+$  mapping with different SNRs.  $SNR_{15}$  is the nominal SNR for  $15^\circ$ , and each plot for a different level of added Gaussian noise is expressed as mean  $\pm$  SD.

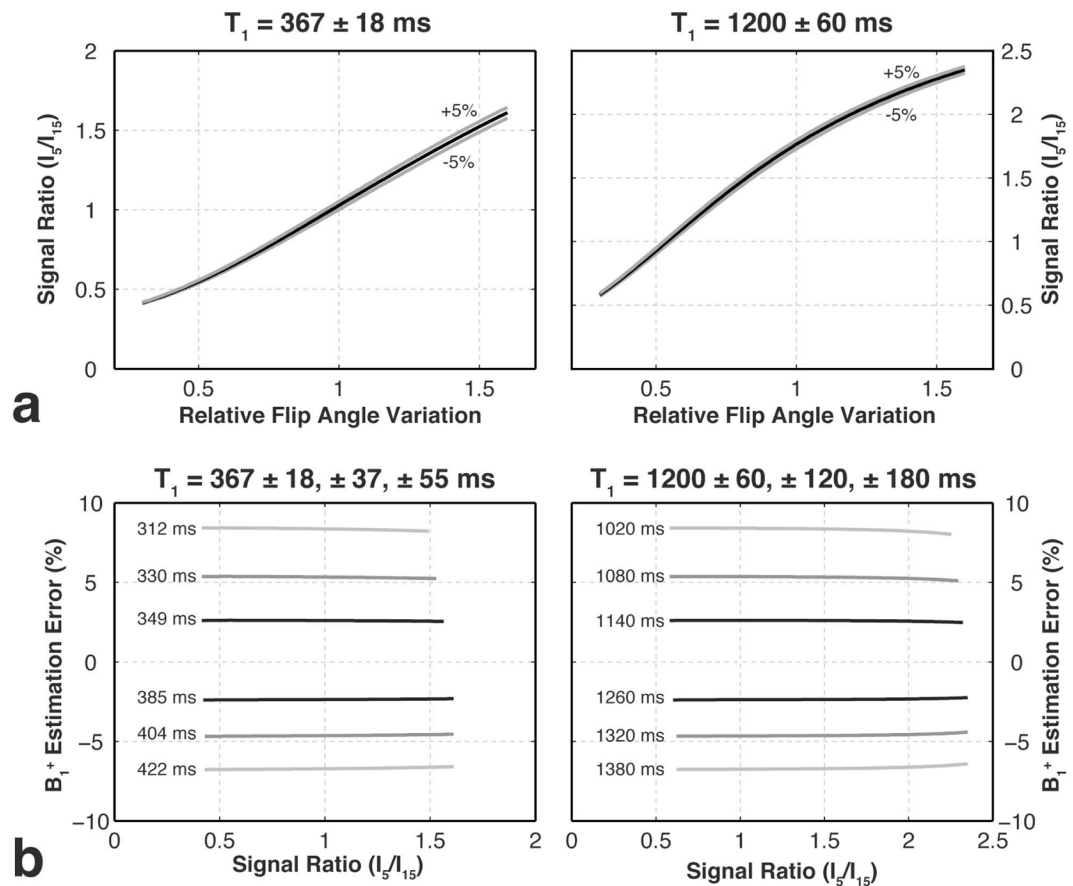


**Figure 4.**

$B_1^+$  estimation errors with different assumed  $T_1$  values in the reference region for a true  $T_1$  of 367 and 1200 ms. (a) The computed signal ratios with  $\pm 5\%$  variations of the true  $T_1$  (gray lines), and (b) the overall  $B_1^+$  estimation errors with different assumed  $T_1$  values ( $\pm 5$ , 10 and 15% variations of the true  $T_1$ ). When the assumed reference  $T_1$  is longer than the true  $T_1$  (positive variations of the true  $T_1$ ), RR-VFA underestimates  $B_1^+$  variation (negative errors).

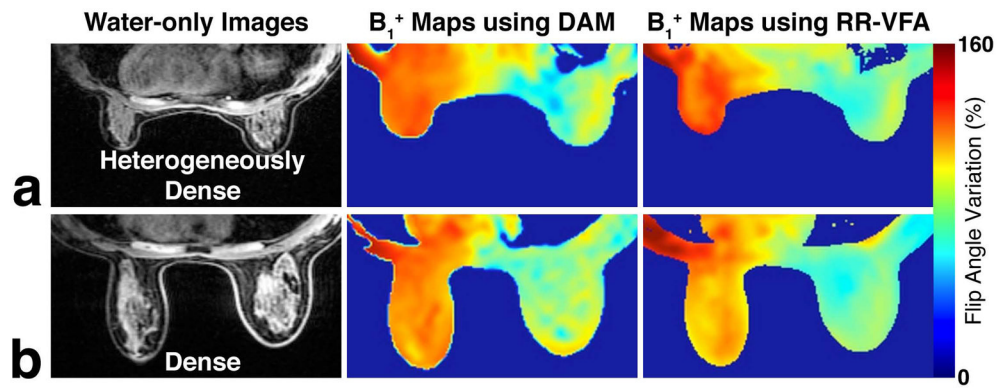


**Figure 5.** Comparison of relative flip angle variation in percentage using DAM and RR-VFA on subjects with (a) heterogeneously dense and (b) dense breasts at 3T. The arrow shows a small region in the heart that does not have enough fatty tissue.

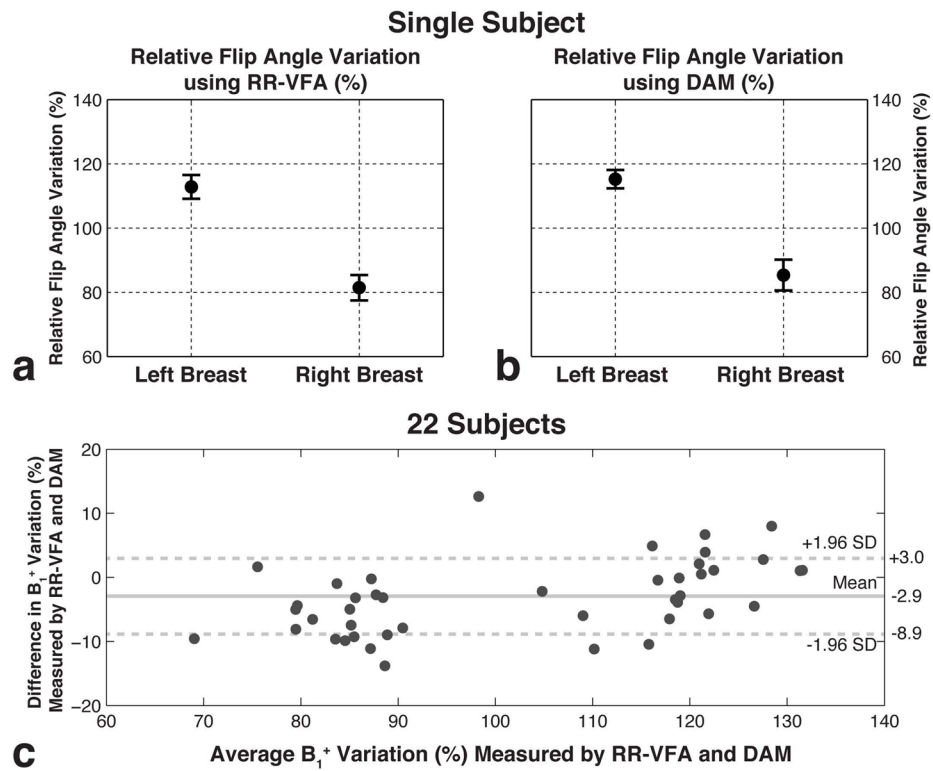


**Figure 6.** Comparison of  $B_1^+$  measurements using RR-VFA and DAM. (a and b) The mean and standard deviation plots for a single subject and (c) the Bland-Altman plot comparing  $B_1^+$  maps in 22 subjects between RR-VFA and DAM methods.

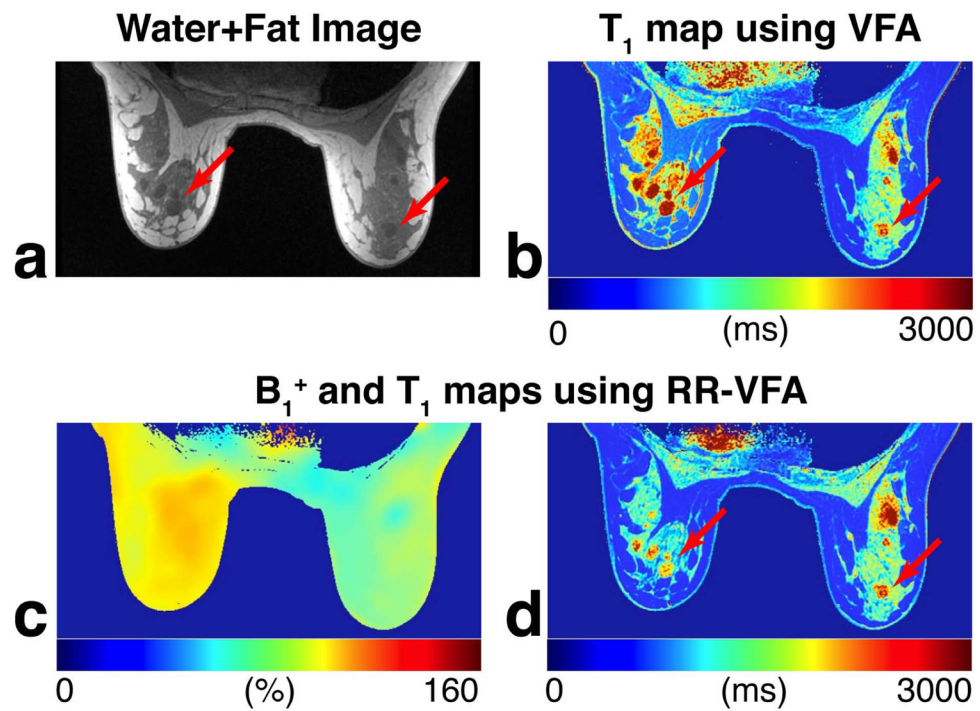


**Figure 7.** High spatial resolution T<sub>1</sub> maps using VFA and RR-VFA. (a) The water+fat image for an anatomical reference, (b) the T<sub>1</sub> map using VFA (without compensating for B<sub>1</sub><sup>+</sup> inhomogeneity), and (c) the estimated B<sub>1</sub><sup>+</sup> map and the T<sub>1</sub> map with compensating for B<sub>1</sub><sup>+</sup> inhomogeneity using RR-VFA. The arrow shows heterogeneous T<sub>1</sub> of several breast masses.



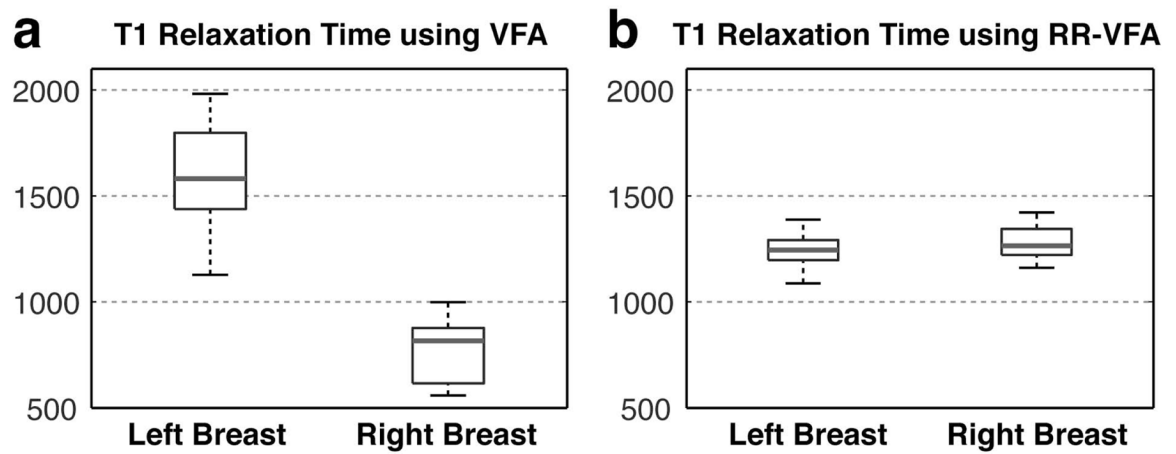


**Figure 8.**

Comparison of  $T_1$  estimation in fibroglandular tissue using (a) standard VFA and (b) RR-VFA with correction of  $B_1^+$  inhomogeneity in 6 breast MRI patients. The central mark on each box is the median, the edges of the box are the 25th and 75th percentiles, and the “whiskers” extend to the most extreme data points that were not considered outliers.